Implementation of the projector augmented-wave LDA+U method: Application to the electronic structure of NiO

O. Bengone,[1,2] M. Alouani,[1] P. Blöchl,[3] and J. Hugel[2]
[1]*Institut de Physique et Chimie des Matériaux de Strasbourg (IPCMS), 23 rue du Loess, F-67037 Strasbourg Cedex, France*
[2]*Univesité de Metz, IPC-LPLI Groupe de Structure Electronique des Milieux Denses, 1 bd Arago, F-57078 Metz Cedex 3, France*
[3]*IBM Research, Zurich Research Laboratory, CH-8803 Rüschlikon, Switzerland*
(Received 20 January 2000)

The so-called local-density approximation (LDA) plus the multiorbital mean-field Hubbard model (LDA+U) has been implemented within the all-electron projector augmented-wave method, and then used to compute the insulating antiferromagnetic ground state of NiO and its optical properties. The electronic and optical properties have been investigated as a function of the Coulomb repulsion parameter U. We find that the value obtained from constrained LDA ($U=8$ eV) is not the best possible choice, whereas an intermediate value ($U=5$ eV) reproduces the experimental magnetic moment and optical properties satisfactorily. At intermediate U, the nature of the band gap is a mixture of charge transfer and Mott-Hubbard type, and becomes almost purely of the charge-transfer type at higher values of U. This is due to the enhancement of the oxygen $2p$ states near the top of the valence states with increasing U value.

I. INTRODUCTION

For many materials, the density-functional theory (DFT)[1] in the local-spin-density approximation (LSDA)[2] provides a good description of their ground-state properties. However, problems arise when the DFT-LSDA approach is applied to materials with ions that contain incomplete d or f shells, such as transition-metal oxides or heavy fermion systems. For example, most transition-metal oxides are wide-gap antiferromagnetic insulators,[3–9] and the DFT-LSDA predicts them to be either metals (FeO and CoO) or small-gap semiconductors (MnO and NiO).[10] The failure of the DFT-LSDA can be traced to the mean-field character of the Kohn-Sham equations as well as to the poor description of strong correlation effects within the homogeneous electron gas. The strong correlation effects are responsible for the breakdown of the DFT-LSDA description of the electronic structure of these compounds. In order to provide a better description of these effects, the Mott-Hubbard picture has been introduced.[11,12]

In the Mott-Hubbard picture of NiO, the d-d Coulomb interaction splits the Ni d sub-bands into the so-called lower and upper Hubbard bands. The upper Hubbard band has mostly Ni $3d^9$ character, while the top of the valence band is of $3d^8$ character, leading to a Mott-Hubbard gap of d-d type. However, O $1s$ x-ray absorption[13] as well as x-ray photoemission and bremsstrahlung isochromat spectroscopies[9] on $Li_xNi_{1-x}O$ have shown that the additional hole has mainly oxygen character. In contrast to the Mott-Hubbard model, the energy-band gap caused by the Ni $3d$ correlations is therefore of the charge-transfer type between the occupied oxygen $2p$ and the Ni $3d$ empty states.

On the other hand, localized approaches,[14–20] such as the local cluster scheme based on the configuration interaction method or the Anderson impurity model, in which transition-metal ions are treated like an impurity in an oxygen $2p$ host, predict a well-defined band gap of 5.0 eV. However, the oxygen $2p$ band dispersion observed in angle-resolved photoemission spectroscopy[21] cannot be described by these methods because the lattice effects are neglected.

Several attempts have been made to include the missing correlation effects in DFT-LSDA. The generalized gradient approximation,[22] which takes into account the radial and angular gradient corrections, can only open a small band gap.[23] The self-interaction correction (SIC)[24–26] eliminates the spurious interaction of an electron with itself from the conventional DFT-LSDA method. Compared to LSDA, the band gap and the magnetic moments are significantly increased. However, the band gap still is too small, and the SIC-LSDA method predicts a larger energy band gap for NiO than for FeO and CoO, in contradiction to experiment.[3] The crystal-field orbital polarization introduced by Norman[27] to determine the magnetism and insulating band gap of transition-metal oxides is promising but underestimates both the spin magnetic moment and the band gap.

Another promising approach for correlated materials is the so-called local-density approximation (LDA) plus the multiorbital mean-field Hubbard model (LDA+U)[28–35] which includes the on-site Coulomb interaction in the LSDA Hamiltonian. After adding the on-site Coulomb interaction to the LSDA Hamiltonian, the potential becomes spin *and* orbital dependent. Because a larger energy cost is associated with fluctuations of the d occupancy, the orbital-dependent potential reduces the fluctuations of the d occupancy, resulting in a better justification of a mean-field approach. LDA+U, although it is a mean-field approach, has the advantage of describing both the chemical bonding and the electron-electron interaction.

The question regarding the best value for the Coulomb repulsion parameter U is, however, still under debate. The U parameter for NiO obtained from a constrained LDA calculation is about 7 to 8 eV, and this is the value generally used in LDA+U calculations. A similar value of U has beenobtained from a constrained LDA calculation for bulk Fe,[29]even though a much smaller value had been expected because of the metallic screening in Fe. The authors argued[29]

that the higher value could be an artifact due to the poor screening within the atomic sphere approximation (ASA), and that within a full-potential calculation a much smaller value of less than 4 eV would be expected. In contrast, an unpublished full-potential linear muffin-tin orbital method calculation by Alouani and Wills[36] clearly shows that the value of U for bulk Fe is even slightly larger than the ASA value. Furthermore, Bulut *et al.*[37] showed that the renormalization of the Coulomb interaction depends on the type of model used. As LDA is not a diagrammatic method, it is not known which type of renormalization is the most appropriate for the LDA+U model. In fact, they found[37] that for an random-phase approximation (RPA) calculation of the spin susceptibility and the self-energy based on the Hubbard model to agree with the full-scale quantum Monte Carlo (QMC) results the U parameter has to be renormalized to $2t$ from its $4t$ value used in the QMC (t being the hopping parameter). It is then clear that the value of U depends on the type of model used to describe the experimental results. As LDA+U is much closer to an RPA type of approach than to a QMC one, the value of U used in the LDA+U method should be much smaller than what QMC will need to reproduce the experiment. If we believe that the QMC will need the experimental U value to describe the experiment, then the value of U used in an LDA+U type of approach should be much smaller than the experimental value.

In this paper we shed light on this problem by treating the Coulomb repulsion parameter U as adjustable parameter, and by investigating how the electronic and optical properties depend on its value. We show that for an intermediate value of $U=5$ eV, good agreement with the measured ground-state antiferromagnetic magnetic moment and optical properties is obtained. We also show that the O $2p$ character near the top of the valence states is enhanced for a larger value of U. Our calculation seems to indicate that the nature of the band gap at intermediate U is a mixture of charge transfer and Mott-Hubbard type, and that it becomes almost purely of the charge-transfer type for higher values of U.

Our calculations are based on the projector augmented-wave (PAW) method,[38] an efficient all-electron method without shape approximations on the potential or electron density to avoid uncertainties due to the ASA approach. Based on a Car-Parrinello-like formalism,[39] the PAW method allows complex relaxations and dynamical properties in strongly correlated systems to be studied. Our implementation of LDA+U within the PAW method is described in detail. Furthermore we discuss possible extensions of the existing method that will enhance its applicability.

The paper is organized as follows: In Sec. II we present those aspects of the PAW formalism that are needed for the implementation of the LDA+U method. In Sec. III we present and discuss the LSDA and LDA+U ground-state properties of NiO, and in Sec. IV we study the optical properties of NiO, namely, the imaginary part of the dielectric function, and compare the results to experiment.

II. FORMALISM

A. PAW method

The PAW method developed by one of us[38] combines ideas of the pseudopotential (PP) and the linear augmented-plane-wave methods. It is applicable to all elements of the periodic table. The nodal behavior of the wave function is correctly described and, as in the PP method, the forces on the ions are easily expressed.

In the PAW method, the all-electron (AE) crystal wave function is constructed from a pseudo (PS) wave function and atomlike functions localized near the nuclei. The PS wave function $|\tilde{\Psi}\rangle$ coincides with the crystal AE wave function $|\Psi\rangle$ in the interstitial region, i.e., outside the atomic regions. Inside the atomic regions Ω_t, called augmentation regions, the wave function is almost atomlike because the effect of the surrounding crystal is small. Therefore, a natural choice is to use solutions $|\phi_\Lambda\rangle$ of Schrödinger's equation for the isolated atom, the so-called AE partial waves, as a basis set for the augmentation region. Here $\Lambda=\{t,\alpha,l,m\}$ is a global index for the atom t, the angular momentum l, the magnetic quantum number m, and the index α, the energy for which Schrödinger's equation is solved.

To link the expansion in atomlike functions near the nuclei to the PS wave function, we introduce a set of auxiliary functions $|\tilde{\phi}_\Lambda\rangle$, so-called PS partial waves, which are centered on the atom and coincide per construction with the corresponding AE partial waves $|\phi_\Lambda\rangle$ outside their augmentation regions:

$$\phi_\Lambda(\mathbf{r})=\tilde{\phi}_\Lambda(\mathbf{r}) \quad \text{for } r\notin\Omega_t. \tag{1}$$

The coefficients c_Λ of the expansions in AE and PS partial waves are chosen such that the PS partial wave expansion $\Sigma_\Lambda|\tilde{\phi}_\Lambda\rangle c_\Lambda$ cancels out the PS wave function $|\tilde{\Psi}\rangle$ inside the augmentation region. For this purpose we introduce so-called projector functions $\langle\tilde{p}|$ such that

$$\sum_\Lambda |\tilde{\phi}_\Lambda\rangle\langle\tilde{p}_\Lambda|=1, \tag{2}$$

and therefore

$$|\tilde{\Psi}\rangle=\sum_\Lambda |\tilde{\phi}_\Lambda\rangle\langle\tilde{p}_\Lambda|\tilde{\Psi}\rangle \tag{3}$$

for the Hilbert space spanned by the PS partial waves $|\tilde{\phi}_\Lambda\rangle$. Thus we identify the expansion coefficients with $c_\Lambda=\langle\tilde{p}_\Lambda\tilde{\Psi}\rangle$. Equation (2) results in the biorthogonality condition

$$\langle\tilde{p}_\Lambda|\tilde{\phi}_{\Lambda'}\rangle=\delta_{\Lambda,\Lambda'} \tag{4}$$

for the projector functions, which moreover are chosen to be localized within the corresponding augmentation region.

With these conditions, the AE Bloch wave function $\Psi(\mathbf{r})$ can be obtained from the PS wave function $\tilde{\Psi}(\mathbf{r})$ as

$$\Psi(\mathbf{r})=\tilde{\Psi}(\mathbf{r})+\sum_\Lambda [\phi_\Lambda(\mathbf{r})-\tilde{\phi}_\Lambda(\mathbf{r})]\langle\tilde{p}_\Lambda|\tilde{\Psi}\rangle. \tag{5}$$

The first term represents the PS wave function defined over the entire space, which is equal to the AE wave function in the interstitial region, and which is expanded in plane waves. The second term is the AE partial wave expansion, which describes the correct nodal behavior of the wave function in the augmentation region $\Omega_R^t(r \leqslant r_c^t)$. The third term eliminates the spurious contribution of the PS wave function in the augmentation region.

Note that Eq. (3) holds only approximately if the set of PS partial waves is not entirely within the augmentation regions. However, this has the advantage that only those contributions of the PS wave function will be removed that are also replaced by AE partial waves. As a result, the AE wave function converges rapidly with the number of partial waves used and, moreover, it is continuous and differentiable for every truncation of the partial-wave expansion.

Expectation values of any sufficiently local operator A are obtained as

$$\langle\Psi|A|\Psi\rangle=\langle\tilde{\Psi}|A|\tilde{\Psi}\rangle+\sum_{\Lambda,\Lambda'}\langle\tilde{\Psi}|\tilde{p}_\Lambda\rangle(\langle\phi_\Lambda|A|\phi_{\Lambda'}\rangle-\langle\tilde{\phi}_\Lambda|A|\tilde{\phi}_{\Lambda'}\rangle)\langle\tilde{p}_{\Lambda'}|\tilde{\Psi}\rangle. \tag{6}$$

Note that the double sum is diagonal in the site indices t,t'. This equation is exact for a complete set of PS partial waves and rapidly attains the converged result if incomplete. The PAW method provides the freedom to represent a zero operator in the form

$$0=\langle\tilde{\Psi}|B|\tilde{\Psi}\rangle-\sum_{\Lambda,\Lambda'}\langle\tilde{\Psi}|\tilde{p}_\Lambda\rangle\langle\tilde{\phi}_\Lambda|B|\tilde{\phi}_{\Lambda'}\rangle\langle\tilde{p}_{\Lambda'}|\tilde{\Psi}\rangle \tag{7}$$

by any operator B entirely localized within the augmentation region. Equation (7) has the same range of validity as Eq. (6) does and allows a further acceleration of the convergence by using a well-chosen operator B and adding the corresponding zero operator to the expression for the expectation value.

B. The LDA+U total-energy functional

For transition-metal oxides, the d orbitals are well localized and keep a strong atomlike character. Even though LDA provides a good approximation for the average Coulomb energy of the d-d interactions, it fails to describe correctly the strong Coulomb and exchange interaction between electrons in the same d shell. The main intention of LDA+U is to identify these atomic orbitals and to describe their electronic interactions as strongly correlated states. The other orbitals are delocalized and considered to be properly described by the LDA. The procedure is to eliminate the averaged LDA energy contribution of these atomlike orbitals from the LDA total-energy functional E^{LDA}, and to add an orbital- and spin-dependent correction. The total energy within the LDA+U method then has the form

$$\begin{aligned}E=E^{\mathrm{LSDA}}&+\frac{1}{2}\sum_{t,\sigma}\sum_{i,j,k,l}\langle\chi_i^t;\chi_k^t|V_{ee}|\chi_j^t;\chi_l^t\rangle n_{i,j}^{t,\sigma}n_{k,l}^{t,-\sigma}\\&+\frac{1}{2}\sum_{t,\sigma}\sum_{i,j,k,l}(\langle\chi_i^t;\chi_k^t|V_{ee}|\chi_j^t;\chi_l^t\rangle\\&-\langle\chi_i^t;\chi_k^t|V_{ee}|\chi_l^t;\chi_j^t\rangle)n_{i,j}^{t,\sigma}n_{k,l}^{t,\sigma}\\&-\sum_t\left[\frac{1}{2}U\sum_{\sigma,\sigma'}N^{t,\sigma}(N^{t,\sigma'}-\delta_{\sigma,\sigma'})\right.\\&\left.-\frac{1}{2}J\sum_\sigma N^{t,\sigma}(N^{t,\sigma}-1)\right],\end{aligned} \tag{8}$$

where $N^{t,\sigma}=\Sigma_i n_{i,i}^{t,\sigma}$ is the average occupation of the d shell for each spin direction as obtained from the d-orbital occupancies $n_{i,j}^{t,\sigma}$. U and J are the Coulomb self-energy and the exchange parameter, respectively. The expressions $\langle\chi_i^t;\chi_k^t|V_{ee}|\chi_j^t;\chi_l^t\rangle$ are the four-center matrix elements of the screened Coulomb interaction V_{ee}. An additional requirement of the LDA+U approach is that the additional energy is applied only to the valence electrons, which are reoptimized while constrained to remain orthogonal to the core states.

C. Orbital occupations

The orbital density matrix is obtained by projection of the crystal wave function onto the augmentation region:

$$n_{m,m'}^{t,\sigma}=\sum_{n,\mathbf{k}}f_{n,\mathbf{k}}^\sigma\langle\Psi_n^{\mathbf{k},\sigma}|P_{m,m'}^t|\Psi_n^{\mathbf{k},\sigma}\rangle, \tag{9}$$

where $f_{n,\mathbf{k}}^\sigma$ is the Fermi distribution.

Here we choose the projection operators $P_{m,m'}^t$ acting on the Ni d-orbitals in analogy to previous implementations[33] as

$$P_{m,m'}^t(\mathbf{r},\mathbf{r}')=\theta_{\Omega_t}(\mathbf{r})\delta(|\mathbf{r}'-\mathbf{R_t}|-|\mathbf{r}-\mathbf{R_t}|)Y_{d,m}(\hat{\mathbf{r}})Y_{d,m'}^*(\hat{\mathbf{r}}'), \tag{10}$$

where the site index t refers to a particular Ni site, and $|Y_{d,m}(\widehat{\mathbf{r}-\mathbf{R}_t})$ is the spherical harmonic for the d orbital and centered at site t. The step functions $\theta_{\Omega_t}(r)$ are unity for $|r-R_t|<r_c^t$ and zero otherwise. [Note that $\langle\chi|P|\chi'\rangle=\int d\mathbf{r}\int d\mathbf{r}'\chi(\mathbf{r})P(\mathbf{r},\mathbf{r}')\chi'(\mathbf{r}')$.] We used an atom in the $3d^84s^2$ configuration of Ni. The local orbitals $|\chi_m^t\rangle$ have been chosen to be identical to those of the spheridized, nonspin-polarized atoms. The radius r_c^t for Ni has been chosen to be $r_c^t=2.1a_0$, and the PAW atomic overlap inside the augmentation region is $\langle\phi^t|P_{m,m}|\phi^t\rangle=0.942$ for Ni.

In the PAW method we obtain the orbital occupations directly from the PS wave functions $|\tilde{\Psi}_n^{\mathbf{k},\sigma}\rangle$ as

$$n_{m,m'}^{t,\sigma}=\sum_{\mathbf{k},n}\langle\tilde{\Psi}_n^{\mathbf{k},\sigma}|\tilde{P}_{m,m'}^t|\tilde{\Psi}_n^{\mathbf{k},\sigma}\rangle, \tag{11}$$

using the pseudoversion

$$\tilde{P}_{m,m'}^t=\sum_{\Lambda,\Lambda'}|\tilde{p}_\Lambda\rangle\langle\phi_\Lambda|P_{m,m'}^t|\phi_{\Lambda'}\rangle\langle\tilde{p}_{\Lambda'}|+\Delta\tilde{P}_{m,m'}^t \tag{12}$$

of the projection operator $P^t_{m,m'}$. Consistent with the PAW formalism, the small correction

$$\Delta\tilde{P}^t_{m,m'} = P^t_{m,m'} - \sum_{\Lambda,\Lambda'} |\tilde{p}_\Lambda\rangle\langle\tilde{\phi}_\Lambda|P^t_{m,m'}|\tilde{\phi}_{\Lambda'}\rangle\langle\tilde{p}_{\Lambda'}| \tag{13}$$

is ignored in the present calculations because it can be considered the pseudoversion of the zero operator.

D. Coulomb and exchange parameters

The four-center integrals used in the expression of the LDA+U total energy are defined as

$$\langle\chi^t_i;\chi^t_j|V_{ee}|\chi^t_k;\chi^t_l\rangle = \int d\mathbf{r}_1 \int d\mathbf{r}_2 \chi^{t*}_i(\mathbf{r}_1)\chi^{t*}_j(\mathbf{r}_2)v_{ee}(\mathbf{r_1},\mathbf{r_2})\chi^t_k(\mathbf{r}_1)\chi^t_l(\mathbf{r}_2), \tag{14}$$

where $v_{ee}(\mathbf{r},\mathbf{r}')$ is the screened Coulomb interaction between two electrons.

If we choose localized d orbitals that are described by an atomic d-wave function $\chi^t_m(\mathbf{r}) = \chi_d(|\mathbf{r}-\mathbf{R}_t|)Y_{d,m}(\widehat{\mathbf{r}-\mathbf{R}_t})$ with magnetic quantum number m and furthermore assume that the static dielectric function ϵ is constant in space, we can exploit the multipole expansion of $1/|\mathbf{r}_1-\mathbf{r}_2|$:

$$v_{ee}(\mathbf{r}_1,\mathbf{r}_2) = \frac{1}{\epsilon|\mathbf{r}_1-\mathbf{r}_2|} = \frac{1}{\epsilon}\sum_{l=0}^{\infty}\frac{4\pi}{2l+1}\frac{r^l_<}{r^{l+1}_>}\sum_{m=-l}^{+l} Y_{lm}(\mathbf{r_1})Y^*_{lm}(\mathbf{r_2}). \tag{15}$$

Here $r_<$ and $r_>$ denote the smallest and largest values of r_1 and r_2, respectively. Under these assumptions we can transform Eq. (14) into

$$\langle\chi^t_1;\chi^t_3|V_{ee}|\chi^t_2;\chi^t_4\rangle = \sum_{l=0}^{\infty}\frac{4\pi}{2l+1}\sum_{m=-l}^{+l}\langle l_1,m_1|Y_{l,m}|l_2,m_2\rangle \times\langle l_3,m_3|Y^*_{l,m}|l_4,m_4\rangle F^l, \tag{16}$$

where (l_i,m_i) are the angular momenta quantum numbers of $|\chi^t_i\rangle$, $\langle l,m|Y_{l'',m''}|l,m'\rangle$ the Gaunt coefficients, and F^l the so-called screened Slater's integrals. Because of the special properties of the Gaunt coefficients, only F^0,F^2, and F^4 contribute to the Coulomb integrals:

$$F^l = \frac{1}{\epsilon}\int_0^\infty dr_1 \int_0^\infty dr_2 r_1^2 r_2^2 \chi^2_d(r_1)\chi^2_d(r_2)\frac{r^l_<}{r^{l+1}_>}. \tag{17}$$

The parameters U and J are identified with averages of the Coulomb and exchange integrals, which are related to the Slater integrals F^0,F^2, and F^4 by the properties of Clebsch-Gordan coefficients, Eq. (16):

$$U = \frac{1}{(2l+1)^2}\sum_{m,m'}\langle\chi^t_m;\chi^t_{m'}|V_{ee}|\chi^t_m;\chi^t_{m'}\rangle = F^0, \tag{18}$$

$$J = \frac{1}{(2l)(2l+1)}\sum_{m\neq m',m'}\langle\chi^t_m;\chi^t_{m'}|V_{ee}|\chi^t_{m'};\chi^t_m\rangle = \frac{F^2+F^4}{14}. \tag{19}$$

The dielectric constant and therefore the Coulomb and exchange parameters U and J are not known *a priori*. Usually, they are obtained from a constrained DFT calculation.[29] Here, we are interested in how sensitively the results depend on the choice of Coulomb parameters, and which Coulomb parameters will provide the best agreement with reality as probed by optical absorption. Therefore, we adopt the general form for the four-center integrals as function of the U and J suggested by the arguments provided above, and perform calculations for different U values, namely, $U=5$ eV and $U=8$ eV. Because the results are fairly insensitive to the exchange parameter J, we have adopted $J=0.95$ eV from previous constrained LDA calculations.[29] The third mandatory relation is obtained from the work of DeGroot *et al.*,[40] who determined the ratio F^4/F^2 for transition-metal oxides to be between 0.62 and 0.63. We therefore adopt a ratio $F^4/F^2=0.625$.

E. Hamiltonian

The pseudo-Hamiltonian operator

$$\tilde{H}_\sigma = \tilde{H}^{LSDA}_\sigma + \tilde{H}^U_\sigma, \tag{20}$$

which acts on the PS wave functions, is obtained as the derivative of the total-energy functional with respect to the two-center pseudodensity matrix operator $\tilde{\rho}_\sigma = \Sigma_{n,\mathbf{k}}|\tilde{\Psi}^{\mathbf{k},\sigma}_n\rangle f^\sigma_{n,\mathbf{k}}\langle\tilde{\Psi}^{\mathbf{k},\sigma}_n|$. The non-LDA contribution of the LDA+U Hamiltonian is then obtained as the product of the derivative $V^{t,\sigma}_{m,m'}$ of the non-LDA contribution to the total energy and the projection operator $\tilde{P}$, which is the derivative of the occupation with respect to the two-center pseudodensity matrix operator. Thus we obtain

$$\tilde{H}^U_\sigma = \sum_{t,m,m'}\tilde{P}^t_{m,m'}V^{t,\sigma}_{m',m}, \tag{21}$$

where

$$\begin{aligned} V^{t,\sigma}_{m_1,m_2} = &\sum_{m_3,m_4}\langle\chi^t_{m_1};\chi^t_{m_3}|V_{ee}|\chi^t_{m_2};\chi^t_{m_4}\rangle n^{t,-\sigma}_{m_3,m_4} \\ &+\sum_{m_3,m_4}[\langle\chi^t_{m_1};\chi^t_{m_3}|V_{ee}|\chi^t_{m_2};\chi^t_{m_4}\rangle \\ &-\langle\chi^t_{m_1};\chi^t_{m_3}|V_{ee}|\chi^t_{m_4};\chi^t_{m_2}\rangle]n^{t,\sigma}_{m_3,m_4} \\ &-\sum_{\sigma'}\left[U\left(N^{t,\sigma'}-\frac{1}{2}\delta_{\sigma,\sigma'}\right)\right. \\ &\left.-\delta_{\sigma,\sigma'}J\left(N^{t,\sigma'}-\frac{1}{2}\right)\right]\delta_{m_1,m_2}. \end{aligned} \tag{22}$$

The LDA contribution of the pseudo-Hamiltonian has the usual form:[38]

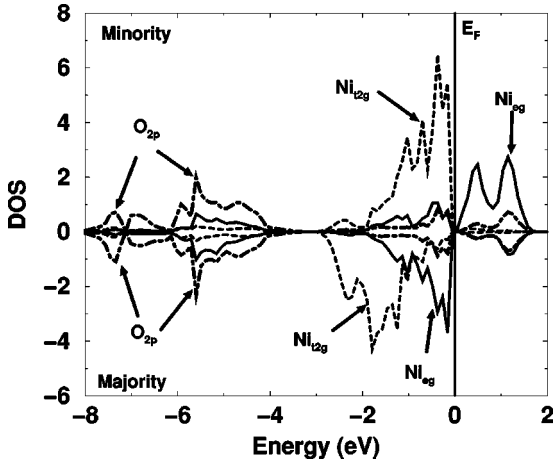

FIG. 1. Atom-resolved antiferromagnetic density of states (DOS, in states per unit cell per eV) of NiO calculated with LSDA. The band gap is, with about 0.1 eV, significantly underestimated. The spin magnetic moment is 0.95 μ_B.

$$\tilde{H}_\sigma^{LDA} = -\frac{\nabla^2}{2} + \tilde{v} + \sum_{\Lambda_1,\Lambda_2} |\tilde{p}_{\Lambda_1}\rangle \Big[\langle \phi_{\Lambda_1}| -\frac{\nabla^2}{2} + v^1 |\phi_{\Lambda_2}\rangle - \langle \tilde{\phi}_{\Lambda_1}| -\frac{\nabla^2}{2} + \tilde{v}^1 |\tilde{\phi}_{\Lambda_2}\rangle \Big] \langle \tilde{p}_{\Lambda_2}|. \quad (23)$$

For the LDA+U calculation, we first performed a self-consistent LSDA calculation using the all-electron PAW method, and then used the self-consistent potential to construct the LSDA Hamiltonian for a large number of **k** points in the Brillouin zone. Next, the Hubbard correction is added to the LSDA Hamiltonian as given by Eq. (20), and the new Hamiltonian iterated until the occupation numbers $n_{m,m'}^{t,\sigma}$ have converged. We have found that the so-called second-variation procedure for self-consistent LDA+U,[33] in which the LSDA potential is updated, did not yield any improvement over our calculations without the update of the LSDA potential. This is consistent with previous LDA+U calculations,[28] as well as with these of Shick *et al.*[33]

III. GROUND STATE OF NiO

A. LSDA ground state

The ground state of NiO has been calculated using the PAW method, and the density-of-states (DOS) is calculated from the self-consistent PAW potential using the tetrahedron method for the Brillouin-zone integration.[41] Figure 1 presents the atom-resolved DOS in the augmentation region. As can be seen, LSDA produced an antiferromagnetic insulating ground state with a small band gap. Table I shows that the LSDA magnetic moment is 0.95 μ_B, and mainly due to the Ni_{e_g} band splitting. This value is much smaller than the experimental value (1.64–1.90 μ_B, Refs. 42 and 43). The calculated band gap of about 0.1 eV is also much smaller than the experimental one (3.0–4.0 eV). The most interesting feature of our LSDA DOS is that the *d* states of Ni dominate the region in the vicinity of the band gap, and that the top of the valence state is of Ni_{e_g} type for the first and $Ni_{t_{2g}}$ type for the second spin. This electronic structure suggests that the band gap is of Mott-Hubbard type. Hence, this LSDA picture of NiO disagrees completely with experiment. It is surprising that the quasiparticle calculation within the so-called GW approximation, performed by Aryasetiawan and Gunnarsson,[44] produced results qualitatively similar to LSDA except for an increased band gap of 6 eV and an increased magnetic moment of 1.6 μ_B. The quantitative change is the reduction of the O $2p$ bandwidth by almost 1 eV (Table I). However, a recent self-consistent model GW calculation by Massida *et al.*,[45] in which the dynamic effects were neglected, produced other results than those of Aryasetiawan and Gunnarsson.[44] It was argued by Massida *et al.* that the results of the former GW calculation are not quite self-consistent, presumably because of the additional nonlocal *ad hoc* potential that is adjusted to the GW calculation in each self-consistent step. The main difference between the two reported GW model calculations is that the latter calculation[45] produced (i) a spreading of the Ni *d* states over the entire valence bandwidth, (ii) a vanishing gap between the O $2p$ and Ni $3d$ and, most importantly, (iii) an enhancement of O $2p$ states at the valence-band maximum. The latter effect attributes the origin of the band gap mainly to a charge transfer gap because this gap is now between the O $2p$ and Ni $3d$ conduction states. Next, we will show that this latter finding is in agreement with the results of the LDA+U model.

B. LDA+U ground state

We have used our implementation of the LDA+U model to determine the ground-state electronic structure of NiO. Although it is common practice to use the *U* extracted from a constrained LDA calculation, we adopt a different point of view here. As stated in the introduction and in agreement with recent results reported in the literature,[46] we believe that the value of *U* extracted from constrained LDA is not the best possible choice. Therefore we have determined the electronic structure of NiO for an intermediate *U* of 5 eV as well as for a larger value of 8 eV.

Figure 2 shows our LDA+U DOS for $U=5$ and 8 eV. The energy-band gap is found to be 2.8 and 4.1 eV, respectively. The total antiferromagnetic spin moment is 1.73 and 1.83 μ_B, respectively. Our DOS obtained for $U=8$ eV

TABLE I. Magnetic moment and band gap of NiO within LDA, LDA+U ($U=5$ eV), and LDA+U ($U=8$ eV). The radii of the augmentation regions are 1.7 and 2.1 a.u. for the oxygen and the nickel atoms, respectively.

	LDA	LDA+U $U=5$ eV	LDA+U $U=8$ eV	Expt.
m (μ_B)	0.95	1.73	1.83	1.64 (Ref. 42)–1.9 (Ref. 43)
gap (eV)	0.1	2.8	4.1	3–4.4

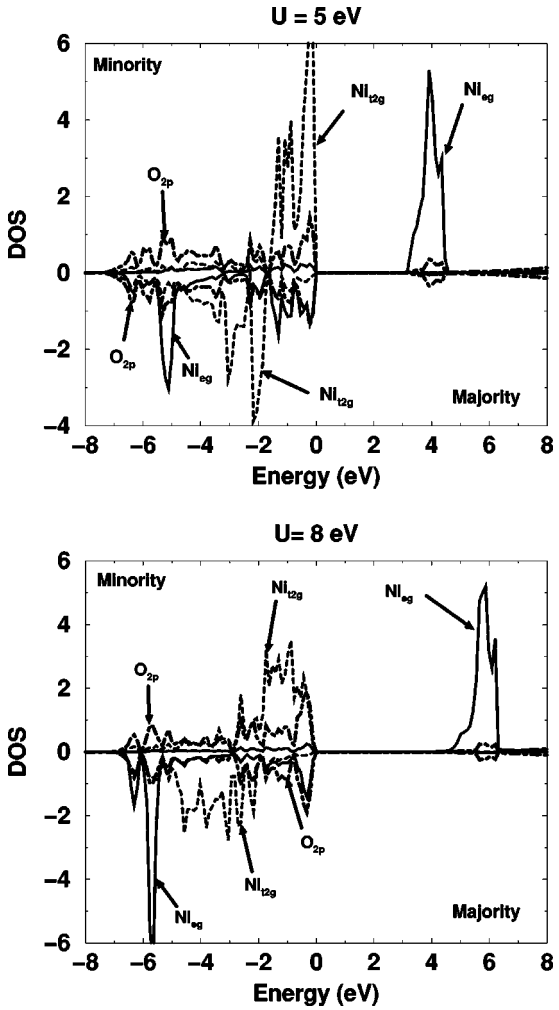

FIG. 2. Atom-resolved density of states (DOS, in states per unit cell per eV) of NiO calculated with LDA+U for (a) $U=5$ eV and (b) $U=8$ eV. The calculated band gap is significantly improved and is ~ 2.8 eV ($U=5$ eV) and 4.1 eV ($U=8$ eV). The antiferromagnetic total magnetic moment of 1.73 μ_B for ($U=5$ eV) and 1.83 μ_B for ($U=8$ eV) is also in good agreement with experiment. The top of the valence state is now O $2p$-like, thus producing a mixed charge-transfer-type band gap.

agrees well with previous LDA+U calculations.[28,32,33,47,48] However, the DOS for $U=5$ eV is in better agreement with the GW model calculation of Massida *et al.*[45] The top of the valence band is reinforced by the O $2p$ states, rendering the band gap a mixture of charge-transfer type and Ni $d \rightarrow d$-like excitations. In agreement with previous LDA+U calculations, the spin majority Ni e_g states are pushed towards lower energies, and the energy difference between $e_g^{\uparrow}$ and $e_g^{\downarrow}$ is about 11 eV for $U=8$ eV and 8.6 eV for $U=5$ eV. Here again the GW model yields a value of about 9 eV for this splitting, in good agreement with our results for $U=5$ eV.

Figure 3 compares our LDA and LDA+U ($U=5$ eV) band structure along the Γ X high-symmetry direction with the available angle-resolved photoemission experiments (ARPES).[21,49] The alignment of experimental and theoretical results has been arbitrarily chosen in order to fit the experimental data to the LDA+U highest valence band at the Γ point. LDA and LDA+U agree well in the low-energy region of the valence band, but the upper valence-band edge

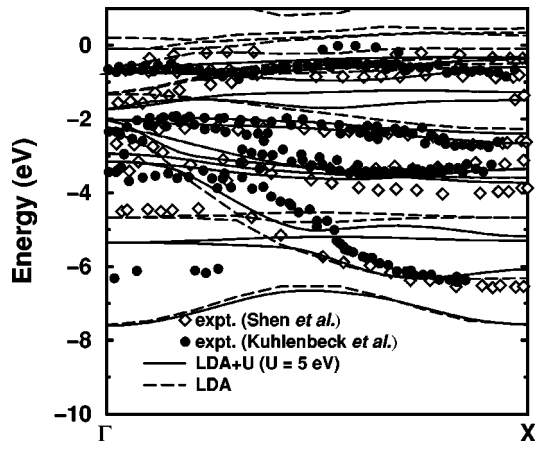

FIG. 3. LSDA (dashed line) and LDA+U ($U=5$ eV) (solid line) calculated band structure along the Γ-X direction compared to the ARPES experiments by Shen *et al.*[21] and by Kuhlenbeck *et al.*[49]

obtained by LDA+U lies about 1 eV below that of LDA. This LDA+U behavior is in agreement with angle-integrated photoemission[8] and O $K\alpha$ x-ray emission spectroscopy,[30] which revealed that whereas the highest-binding-energy (BE) region corresponding to the O $2p$ energy region is correctly described within LSDA (and LDA+U), the Ni $3d$ region at low BE is shifted about 2 eV towards higher energies. The LSDA Ni $3d$ bands should be shifted by about 2 eV towards lower energies to agree with angle-integrated photoemission. Consequently, the fact that the LDA+U Ni $3d$ energy region at low BE is shifted downwards in energy, closer to the O $2p$ region due to the large Hubbard interaction, corresponds to an experimental observation and justifies the choice of aligning the experimental ARPES data with the LDA+U rather than with the LDA bands.

Regarding the details of the comparison with experiment, Fig. 3 shows that our LDA+U results in general are in good agreement with both experimental ARPES data.[21,49] In particular, all data points by Kuhlenbeck *et al.*[49] in the low $[-1;0.5]$ eV region correspond to the LDA+U calculated bands, except for few points in the middle of the Γ-X direction at -0.5 eV. Shen *et al.*[21] distinguished three band components in their experiment in the same energy domain, and some of their points do not agree with our LDA+U calculation, especially the few points at -0.5 eV BE in the first part of the Γ-X direction. However, others points coincide with LDA+U calculated bands. In the $[-3.5;-2]$ eV region, there are a number of data points corresponding to two bands in the experiment of Kuhlenbeck and co-workers and to three bands in that of Shen and co-workers. The first band with lower BE between $[-2.5;-2]$ eV, which is rather flat in both experiments, agrees quite well with LDA+U bands along the entire Γ-X direction. The second band in this energy region, beginning at -2 eV at the Γ point and reaching the X point at -3 eV, is also in agreement with both experiments, except for the points close to the Γ point. In the $[-4;-3]$ eV energy range, Shen *et al.* found a third band, which is was not resolved by Kuhlenbeck *et al.* and is in semiquantitative agreement with the LDA+U bands. The O $2p$ region is quite well described by our LDA+U results, except for the folded-back band at -5.5 eV, located at about

1 eV below the data of Shen *et al.* and 1 eV above that of Kuhlenbeck *et al.* Nevertheless, the latter structure near -7 eV is interpreted by Kuhlenbeck *et al.* as a Ni $3d$ satellite. The disagreement between the folded-back band and the experimental results of Shen *et al.* was interpreted by Massida *et al.*[45] as due to the absence of satellite structures in the one-electron theory.

IV. DIELECTRIC FUNCTION

For insulators, the imaginary part of the macroscopic dielectric function is obtained within the RPA in the long-wavelength limit without local-field effects as[50]

$$\epsilon_2(\omega)=\lim_{q\to 0}\sum_{v,c}\sum_{\mathbf{k}}\frac{8\pi^2}{\Omega q^2}|M^{c,\mathbf{k}}_{v,\mathbf{k}-\mathbf{q}}|^2 f_{v,\mathbf{k}-\mathbf{q}}(1-f_{c,\mathbf{k}}) \times\delta(E^{\mathbf{k}}_c-E^{\mathbf{k}-\mathbf{q}}_v-\hbar\omega). \tag{24}$$

Here $M^{c,\mathbf{k}}_{v,\mathbf{k}-\mathbf{q}}$ are the interband transition matrix elements, $f_{v,\mathbf{k}}$ is the zero-temperature Fermi distribution, Ω is the cell volume, c denotes the conduction-band and v the valence-band index. In the case of a local potential, the interband transition matrix elements are given by

$$\lim_{q\to 0} M^{c,\mathbf{k}}_{v,\mathbf{k}-\mathbf{q}}=\frac{\mathbf{q}}{\epsilon_{c,\mathbf{k}}-\epsilon_{v,\mathbf{k}}}\langle\Psi^{\mathbf{k}}_v|\mathbf{p}|\Psi^{\mathbf{k}}_c\rangle, \tag{25}$$

where the matrix elements $\langle\Psi^{\mathbf{k}}_v|\mathbf{p}|\Psi^{\mathbf{k}}_c\rangle$ are calculated using the PAW crystal wave functions $\Psi^{\mathbf{k}}$ described by Eq. (5):

$$\langle\Psi^{\mathbf{k}}_v|\mathbf{p}|\Psi^{\mathbf{k}}_c\rangle=\langle\tilde{\Psi}^{\mathbf{k}}_v|\mathbf{p}|\tilde{\Psi}^{\mathbf{k}}_c\rangle+\sum_{\Lambda,\Lambda'}\langle\tilde{\Psi}^{\mathbf{k}}_v|\tilde{p}_\Lambda\rangle[\langle\phi_\Lambda|\mathbf{p}|\phi_{\Lambda'}\rangle -\langle\tilde{\phi}_\Lambda|\mathbf{p}|\tilde{\phi}_{\Lambda'}\rangle]\langle\tilde{p}_{\Lambda'}|\tilde{\Psi}^{\mathbf{k}}_c\rangle. \tag{26}$$

In the most general case, i.e., where the potential is nonlocal as in LDA+U, a nonlocal contribution has to be added to the interband transition matrix elements.[51] The full derivation is given in the appendix by Eq. (A6). For NiO, the nonlocal contribution to the matrix elements is found to be small, i.e., of a few percent.

Figure 4 shows the imaginary part of the dielectric function calculated within the LSDA. The resulting optical spectrum is not in agreement with experiment (see Fig. 5). In particular, the optical gap is considerably underestimated and the first structure has a much higher intensity compared to experiment. Conversely, for $U=5$ eV, our calculated imaginary part of the dielectric function within the LDA+U is in a better agreement with experiment, as shown in Fig. 5. The optical band gap and the oscillator strength of the first excitation peak are in excellent agreement with experiment. However, at higher-photon energies the agreement with experiment is only qualitative, which is expected owing to the mean-field approximation of this simple model. A much higher value of U, i.e., 8 eV, produces a much larger optical gap in contrast to experiment. In agreement with our conclusion that a much smaller value of U is required to describe NiO, Dudarev and co-workers[46] also found that $U=6.2$ eV reproduces the lattice parameter and the measured electron-energy loss spectra. It is too early to draw a definitive conclusion about the excited states of NiO, as our LDA+U model is a mean-fieldlike model in which excitonic effects are not included. To our knowledge, no calculations of excitonic effects have so far been attempted. Our results represent the first investigation of the low-lying excited states of NiO that considers all the subtleties of chemical bonding *and* strong electron-electron interaction.

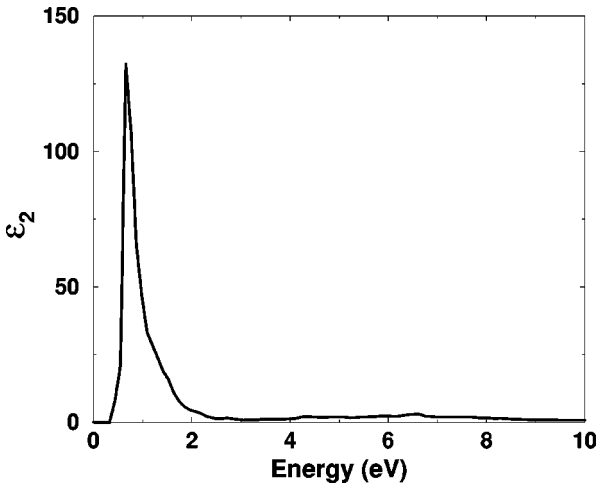

FIG. 4. LSDA calculated imaginary part of the dielectric function $\epsilon_2(\omega)$ of NiO. Compared to experiment, the optical energy gap is underestimated and the first excitation peak is very intense. This intense peak is due to interband transitions from the top of the valence band of O $2p$ character to the bottom of the conduction band of type Ni e_g character.

The interband transitions are responsible for the first structure in the optical spectrum of NiO, located between 4.1 and 5 eV. We found that 40.2% of the contribution results from the transition from band 15 (second highest-occupied band) to band 17 (lowest empty band), 36.2% from the transition 16→18, and 15.9% from the interband transition 16

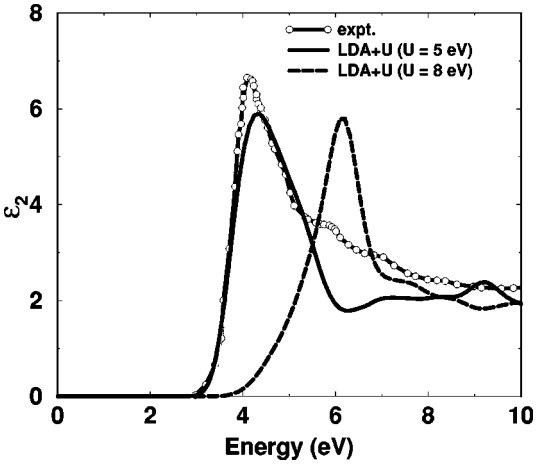

FIG. 5. Calculated LDA+U imaginary part of the dielectric function of NiO convoluted with a Gaussian lifetime at half maximum of 0.3 eV for $U=5$ eV (solid curve) and for $U=8$ eV (dashed curve) compared to the experimental optical spectrum[3] (dashed-dotted curve). The agreement with experiment is much better for $U=5$ eV. Most of the interband transitions giving rise to the first peak are from the top of the valence band of O 2 character to the bottom of the conduction band of Ni e_g character. At higher photon energy, the disagreement becomes stronger.

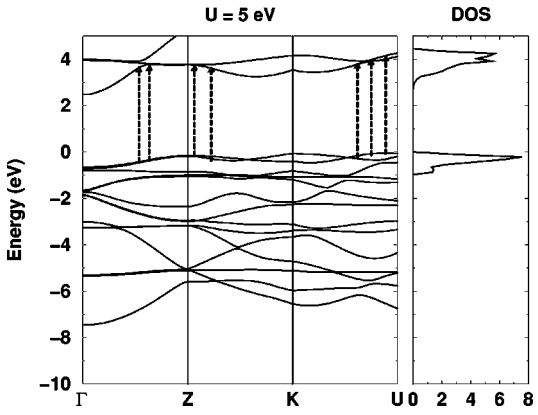

FIG. 6. Left panel: band structure of NiO calculated with LDA+U for $U=5$ eV along the high-symmetry directions ΓZ, ZK, and KU. Right panel: density of states (DOS, in states per unit cell per eV) of the initial and final states responsible for the first peak of the imaginary part of the dielectric function. The interband transitions between parallel bands giving rise to the first optical peak are indicated by arrows.

$\rightarrow$17. To analyze the character of the initial and final states of the interband transitions, the band-structure dispersion along some of the high-symmetry directions is shown in Fig. 6 together with the DOS of the states that give rise to the first optical peak. The arrows between the parallel bands indicate the interband transitions from the initial to the final state responsible for the first structure in the optical spectrum. Figure 7 shows the charge density plot of the initial and final states $\Psi_n^{\mathbf{k},\sigma}$ for bands 16 (highest occupied band) and 18 (second lowest empty band) at point $\mathbf{k}=(127/120,127/360,\sqrt{3}/90)\pi/a$ located between the high-symmetry points K and U, where the optical matrix element value is among the largest. It also shows that the initial state is of mixed O $2p$ and Ni $3d$ character, whereas the final state mainly is of Ni e_g character. The optical transitions then are between the O $2p$ and the Ni $3d$ states, resulting in excitations of the charge-transfer type. Our interpretation differs from that of Fujimori and Minami,[14] who used a configuration interaction within the metal-ligand cluster and claimed that the $d\rightarrow d$ charge-transfer transitions are the origin of fundamental edge. The drawback of the cluster calculation is that in reality the oxygen $2p$ orbitals are delocalized and therefore not well described in a small cluster. On the other hand, an earlier, band-structure-based interpretation by Messick and co-workers[4] assigned the peak to one-electron interband transitions associated with Ni $3d$ to the Ni $4s$ states. This interpretation is not correct either because the Ni $4s$ are far above the top of the valence states (greater than 6 eV), and only quadrupolar interband transitions are permitted between the $3d$ and $4s$ states, which substantially reduces the peak intensity.

V. CONCLUSION

We have presented a new implementation of LDA+U model based on the PAW method,[38] which is an all-electron method without any shape approximation to the potential or the charge density. We tested the method on NiO and obtained results that are in good agreement with previous

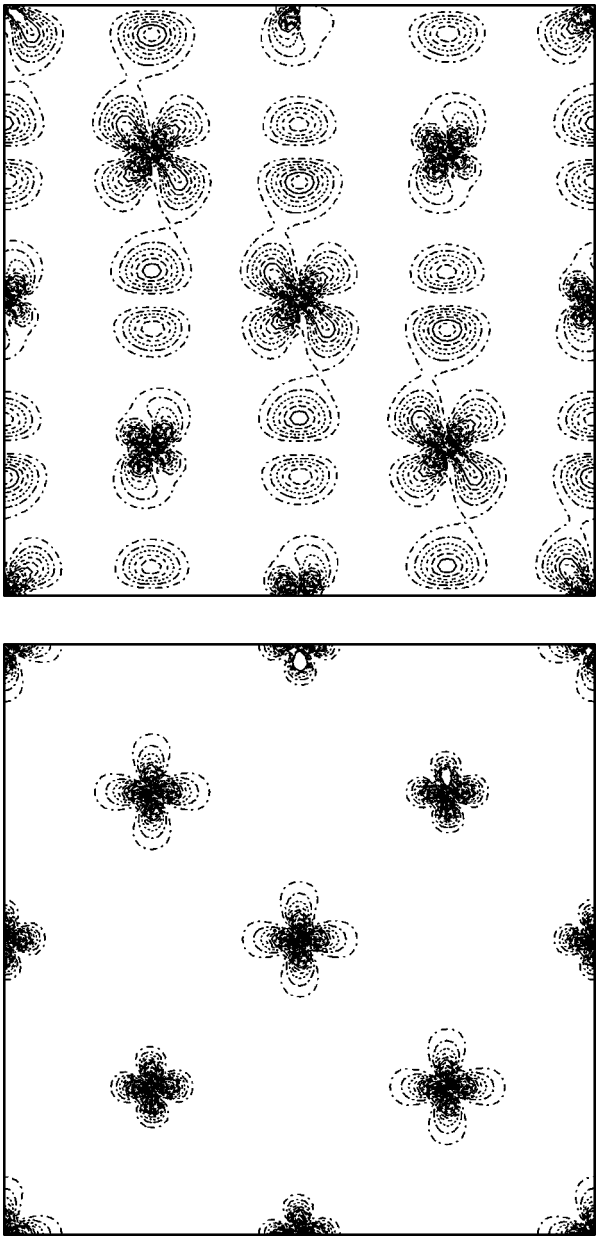

FIG. 7. Initial (top) and final (bottom) charge densities of one spin direction at the point $\mathbf{k}=(127/120,127/360,\sqrt{(3)}/90\pi a$ located between the high-symmetry points K and U of the topmost valence band (16) and the second lowest conduction band (18), where the optical matrix element value is among the largest. The interband transitions giving rise to the first peak of the optical spectrum of NiO are due to allowed electronic transition between initial O $2p$ and Ni e_g final states as shown in the plot.

LDA+U calculations and a recent GW model calculation.[45] In particular, we obtained the correct antiferromagnetic insulating ground state of NiO.

We discussed the results in terms of the strength of the Hubbard interaction U. The optimum value of U has been determined by comparison with the experimental dielectric function as well as with the ground-state properties. We observed a large enhancement of the O $2p$ character at the top of the valence state, resulting in a more charge-transfer than Ni $d\rightarrow d$ LSDA-type band gap. The calculated antiferromagnetic moment is in good agreement with experiment.

Our calculated dielectric function for an intermediate value of U, namely, 5 eV, is in good agreement with experiment. The low-lying, strong structure in the optical spectrum has been assigned to an interband transition from O $2p$ states at top of the valence band to the Ni e_g states at the conduction-band bottom. Hence the origin of the first optical peak is due to a charge-transfer excitation.

Our calculation is supported by a recent LDA+U calculation by Dudarev and co-workers,[46] who also argue that a much smaller value of U than the one obtained from constrained LDA calculation is needed to describe the electron energy-loss spectra and the equilibrium lattice parameter. It should be interesting to apply this method to other transition-metal oxides and check the applicability of LSDA+U for producing excitation energies.

ACKNOWLEDGMENTS

Part of this work was done during our (O.B. and M.A.) visit to the Ohio State University in the summer of 1998. We thank J. W. Wilkins and J. G. LePage for useful discussions. Supercomputer time was provided by CINES (project gem1101) on the IBM SP2 and by the Université Louis Pasteur on the SGI O2000 supercomputer.

APPENDIX: OPTICAL TRANSITION MATRIX ELEMENTS IN LDA+U

The interband transition matrix elements for a given Hamiltonian are obtained as follows:

$$\begin{aligned} M_{v,\mathbf{k}-\mathbf{q}}^{c,\mathbf{k}} &= \langle \Psi_{v,\mathbf{k}-\mathbf{q}} | e^{-i\mathbf{q}\mathbf{r}} | \Psi_{c,\mathbf{k}} \rangle \\ &= \frac{\langle \Psi_{v,\mathbf{k}-\mathbf{q}} | (\epsilon_{v,\mathbf{k}-\mathbf{q}} - \epsilon_{c,\mathbf{k}}) e^{-i\mathbf{q}\mathbf{r}} | \Psi_{c,\mathbf{k}} \rangle}{\epsilon_{v,\mathbf{k}-\mathbf{q}} - \epsilon_{c,\mathbf{k}}} \\ &= \frac{\langle \Psi_{v,\mathbf{k}-\mathbf{q}} | H e^{-i\mathbf{q}\mathbf{r}} - e^{-i\mathbf{q}\mathbf{r}} H | \Psi_{c,\mathbf{k}} \rangle}{\epsilon_{v,\mathbf{k}-\mathbf{q}} - \epsilon_{c,\mathbf{k}}} \\ &= \frac{\langle \Psi_{v,\mathbf{k}-\mathbf{q}} | [H, e^{-i\mathbf{q}\mathbf{r}}]_- | \Psi_{c,\mathbf{k}} \rangle}{\epsilon_{v,\mathbf{k}-\mathbf{q}} - \epsilon_{c,\mathbf{k}}}. \end{aligned} \tag{A1}$$

The commutator involving of the LDA contribution H^{LDA} to the Hamiltonian $H = H^{\mathrm{LDA}} + H^U$ is

$$\begin{aligned} [H^{\mathrm{LDA}}, e^{-i\mathbf{q}\mathbf{r}}]_- &= -\frac{1}{2}[\nabla^2, e^{-i\mathbf{q}\mathbf{r}}]_- \\ &= -\frac{1}{2}(-2i\mathbf{q}\nabla + q^2) \\ &= -\mathbf{q}\mathbf{p} + O(q)^2. \end{aligned} \tag{A2}$$

The quadratic and higher-order terms in $\mathbf{q}$ can be ignored in the long-wavelength limit appropriate for optical transitions. The commutator involving the non-LDA part H^U is obtained as

$$\begin{aligned} [H^U, e^{-i\mathbf{q}\mathbf{r}}]_- &= -i\mathbf{q}[H^U, \mathbf{r}]_- + O(q)^2 \\ &= -i\mathbf{q} \sum_{t,m,m'} V^t_{m,m',\sigma} [P^t_{m',m}, \mathbf{r}]_- + O(q)^2. \end{aligned} \tag{A3}$$

Next we use the relation that holds for the special form of the projector operator presented in Eq. (10)

$$P^{t'}_{m'',m'} | \phi_{t,l,m,\alpha} \rangle = \theta_{\Omega_t}(\mathbf{r}) | \phi_{t,l,m'',\alpha} \rangle \delta_{t,t'} \delta_{l,2} \delta_{m,m'}, \tag{A4}$$

i.e., the projection operator changes the magnetic quantum number of a specific d-like partial wave from m to m'' and truncates it beyond the atomic sphere Ω_t. Hence we obtain

$$\begin{aligned} \langle \phi_\Lambda | [P^t_{m',m}, \mathbf{r}]_- | \phi^t_{\Lambda'} \rangle &= \langle P^{t\dagger}_{m',m} \phi_\Lambda | \theta_{\Omega_t}(\mathbf{r}) \mathbf{r} | \phi_{\Lambda'} \rangle \\ &\quad - \langle \phi_\Lambda | \theta_{\Omega_t}(\mathbf{r}) \mathbf{r} | P^t_{m,m'} \phi_{\Lambda'} \rangle. \end{aligned} \tag{A5}$$

Finally, we obtain the expression of the matrix elements for the dipole transition, with the PAW LDA+U formalism:

$$\begin{aligned} \lim_{q\to 0} M_{v,\mathbf{k}-\mathbf{q}}^{c,\mathbf{k}} = \frac{-\mathbf{q}}{(\epsilon_{v,\mathbf{k}-\mathbf{q}} - \epsilon_{c,\mathbf{k}})} \Bigg\{ & \langle \tilde{\Psi}_{v,\mathbf{k}} | \mathbf{p} | \tilde{\Psi}_{c,\mathbf{k}} \rangle \\ & + \sum_{\Lambda,\Lambda'} \delta_{t,t'} \langle \tilde{\Psi}_{v,\mathbf{k}} | \tilde{p}_\Lambda \rangle \Big[\langle \phi_\Lambda | \mathbf{p} | \phi_{\Lambda'} \rangle \\ & - \langle \tilde{\phi}_\Lambda | \mathbf{p} | \tilde{\phi}_{\Lambda'} \rangle \\ & + i \sum_{m,m'} V^t_{m,m'} (\langle P^{t\dagger}_{m,m'} \phi_\Lambda | \theta_{\Omega_t}(\mathbf{r}) \mathbf{r} | \phi_{\Lambda'} \rangle \\ & - \langle \phi_\Lambda | \theta_{\Omega_t}(\mathbf{r}) \mathbf{r} | P^t_{m,m'} \phi_{\Lambda'} \rangle) \Big] \langle \tilde{p}_{\Lambda'} | \tilde{\Psi}_{c,\mathbf{k}} \rangle \Bigg\}. \end{aligned} \tag{A6}$$

The difference between wave functions $|\tilde{\Psi}_{v,\mathbf{k}}\rangle$ and $|\tilde{\Psi}_{v,\mathbf{k}-\mathbf{q}}\rangle$ has been ignored because it only contributes to terms that are proportional to q^2, which are ignored in the long-wavelength limit.

[1] P. Hohenberg and W. Kohn, Phys. Rev. **136**, B864 (1964).
[2] W. Kohn and L. J. Sham, Phys. Rev. **140**, A1133 (1965).
[3] R. Powell and W. E. Spicer, Phys. Rev. B **2**, 2185 (1970).
[4] L. Messick, W. C. Walker, and R. Glosser, Phys. Rev. B **6**, 3941 (1972).
[5] G. A. Sawatzky and J. W. Allen, Phys. Rev. Lett. **53**, 2239 (1984).
[6] S. Hüfner, P. Steiner, I. Sander, F. Reinert, and H. Schnitt, Z. Phys. B: Condens. Matter **86**, 207 (1992).
[7] S. Hüfner, Solid State Commun. **53**, 707 (1985).
[8] S. Hüfner, J. Osterwaldr, T. Riesterer, and F. Hullinger, Solid State Commun. **52**, 793 (1984).
[9] J. van Elp, H. Eskes, P. Kuiper, and G. A. Sawatzky, Phys. Rev. B **45**, 1612 (1992), and references therein.

[10] K. Terakura, T. Oguchi, A. R. Williams, and J. Kübler, Phys. Rev. B **30**, 4734 (1984).
[11] N. F. Mott, Proc. R. Soc. London, Ser. A **42**, 416 (1949).
[12] J. Hubbard, Proc. R. Soc. London, Ser. A **276**, 238 (1963).
[13] P. Kuiper, G. Kruizinga, J. Ghijsen, G. A. Sawatzky, and H. Verweij, Phys. Rev. Lett. **62**, 221 (1989).
[14] A. Fujimori, F. Minami, and S. Sugano, Phys. Rev. B **29**, 5225 (1984); A. Fujimori and F. Minami, *ibid.* **30**, 957 (1984).
[15] G. J. M. Janssen and W. C. Nieuwpoort, Phys. Rev. B **38**, 3449 (1988).
[16] K. Okada and A. Kotani, J. Phys. Soc. Jpn. **61**, 4619 (1992).
[17] H. Zheng, Phys. Rev. B **48**, 14 868 (1993).
[18] G. A. Benesh and D. E. Ellis, Phys. Rev. B **24**, 1603 (1981).
[19] A. Tanaka and T. Jo, J. Phys. Soc. Jpn. **63**, 2788 (1994).
[20] J. Zaanen, G. A. Sawatzky, and J. W. Allen, Phys. Rev. Lett. **55**, 418 (1985).
[21] Z.-X. Shen, C. K. Shih, O. Jepsen, W. E. Spicer, I. Lindau, and J. W. Allen, Phys. Rev. Lett. **64**, 2442 (1990); Z-X. Shen, J. W. Allen, P. A. P. Lindberg, D. S. Dessau, B. O. Wells, A. Borg, W. Ellis, J. S. Kang, S-J. Oh, I. Lindau, and W. E. Spicer, Phys. Rev. B **42**, 1817 (1990); Z-X. Shen, R. S. List, D. S. Dessau, B. O. Wells, O. Jepsen, A. J. Arko, R. Barttlet, C. K. Shih, J. C. Huang, and P. A. P. Lindberg, *ibid.* **44**, 3604 (1991).
[22] J. P. Perdew, J. A. Chevary, S. H. Vosko, K. A. Jackson, M. R. Pederson, D. J. Singh, and C. Fiolhais, Phys. Rev. B **46**, 6671 (1992).
[23] P. Dufek, P. Blaha, V. Sliwko, and K. Schwarz, Phys. Rev. B **49**, 10 170 (1994).
[24] A. Svane and O. Gunnarsson, Phys. Rev. Lett. **65**, 1148 (1990).
[25] Z. Szotek and W. M. Temmerman, Phys. Rev. B **47**, 4029 (1993).
[26] M. Arai and T. Fujiwara, Phys. Rev. B **51**, 1477 (1995).
[27] M. R. Norman, Phys. Rev. B **44**, 1364 (1991).
[28] V. I. Anisimov, J. Zaanen, and O. K. Andersen, Phys. Rev. B **44**, 943 (1991); V. I. Anisimov, M. A. Korotin, J. Zaanen, and O. K. Andersen, Phys. Rev. Lett. **68**, 343 (1992); V. I. Anisimov, I. V. Solovyev, M. A. Korotin, M. T. Czyzyk, and G. A. Sawatzky, Phys. Rev. B **48**, 16 929 (1993).
[29] V. I. Anisimov and O. Gunnarsson, Phys. Rev. B **43**, 7570 (1991).
[30] V. I. Anisimov, P. Kuiper, and J. Nordgren, Phys. Rev. B **50**, 8257 (1994).
[31] W. E. Pickett, S. C. Erwin, and E. C. Ethridge, Phys. Rev. B **58**, 1201 (1998).
[32] S. L. Dudarev, A. I. Liechtenstein, M. R. Castell, G. A. D. Briggs, and A. P. Sutton, Phys. Rev. B **56**, 4900 (1997).
[33] A. B. Shick, A. I. Liechtenstein, and W. E. Pickett, Phys. Rev. B **60**, 10 763 (1999).
[34] I. V. Solovyev, P. H. Dederichs, and V. I. Anisimov, Phys. Rev. B **43**, 16 861 (1994).
[35] A. I. Liechtenstein, V. I. Anisimov, and J. Zaanen, Phys. Rev. B **52**, R5467 (1995).
[36] M. Alouani and J. M. Wills (unpublished).
[37] N. Bulut, D. J. Scalapino, and S. R. White, Phys. Rev. B **47**, 2742 (1993).
[38] P. E. Böchl, Phys. Rev. B **50**, 17 953 (1994).
[39] R. Car and M. Parrinello, Phys. Rev. B **55**, 2471 (1985).
[40] F. M. de Groot, J. C. Fuggle, B. T. Thole, and G. A. Sawatzky, Phys. Rev. B **42**, 5459 (1990).
[41] O. Jepsen and O. K. Andersen, Solid State Commun. **9**, 1763 (1971); G. Lehmann and M. Taut, Phys. Status Solidi **54**, 469 (1972).
[42] H. A. Alperin, J. Phys. Soc. Jpn. **17**, 12 (1962).
[43] A. K. Cheetham and D. A. Hope, Phys. Rev. B **27**, 6964 (1983).
[44] F. Aryasetiawan and O. Gunnarsson, Phys. Rev. Lett. **74**, 3221 (1995).
[45] S. Massida, A. Continenza, M. Posternak, and A. Baldereschi, Phys. Rev. B **55**, 13 494 (1997).
[46] S. L. Dudarev, G. A. Botton, S. Y. Savrasov, C. J. Humphreys, and A. P. Sutton, Phys. Rev. B **57**, 1505 (1998).
[47] P. Wei and Z. Q. Qi, Phys. Rev. B **49**, 10 864 (1994).
[48] J. Hugel and M. Kamal, J. Phys.: Condens. Matter **9**, 647 (1997).
[49] H. Kuhlenbeck, G. Odörfer, R. Jaeger, G. Illing, M. Menges, Th. Mull, H.-J. Freund, M. Pöhlchen, V. Staemmler, S. Witzel, C. Scharfschwerdt, K. Wennemann, T. Liedtke, and M. Neumann, Phys. Rev. B **43**, 1969 (1991).
[50] H. Ehrenreich and M. L. Cohen, Phys. Rev. **115**, 786 (1959).
[51] M. S. Hybertsen and S. G. Louie, Phys. Rev. B **35**, 5585 (1987).